Influence of modern machining processes on the surface integrity of high-entropy alloys

IOP Conf. Series: Materials Science and Engineering **882** (2020) 012016 doi:10.1088/1757-899X/882/1/012016

Influence of modern machining processes on the surface integrity of high-entropy alloys

T Richter[1], D Schröpfer[1], M Rhode[1,2] and A Börner[1]

[1] Department 9 - Component Safety, Bundesanstalt für Materialforschung und -prüfung (BAM), Unter den Eichen 87, 12205 Berlin, Germany
[2] Institute for Materials and Joining Technology, Faculty of Mechanical Engineering, Otto-von-Guericke-University, Universitätsplatz 2, 39106 Magdeburg, Germany

tim.richter@bam.de

Abstract. High Entropy Alloys (HEAs) are a recent class of materials. In contrast to conventional alloys, HEAs consist of five alloying elements in equiatomic equilibrium. The high entropy effect is due, among other things, to the increased configuration entropy, which promotes solid solution formation. Many HEAs have enormous application potential due to excellent structural property combinations from very low to high temperatures. For the introduction of HEAs in real components, however, the question of the applicability of machining production technologies for component manufacture is of central importance. This has so far received little attention in global materials research. Reliable and safe processing is essential for the demand of economical component production for potential areas of application, e.g. in power plant technology. For metals, milling is the standard machining process. This article presents the results of machining analyses. It focuses on the surface integrity resulting from the milling process on a $Co_{20}Cr_{20}Fe_{20}Mn_{20}Ni_{20}$-HEA. For this purpose, investigations were carried out using ball nose end milling tools for conventional milling process in comparison to an innovative hybrid process available at BAM Berlin, Ultrasonic-Assisted Milling (USAM). USAM promises a lower degradation of the surface properties due to lower loads on the workpiece surface during machining. For this purpose, basic milling parameters (cutting speed and tooth feed) were systematically varied and cutting forces were measured during the milling experiments. The subsequent analysis of these forces allows an understanding of the mechanical loads acting on the tool and component surface. These loads cause topographical, mechanical and microstructural influences on the surface and consequently on the surface integrity. For their characterization, light and scanning electron microscopy were used, and the roughness and residual stresses via X-ray diffraction were measured. The results indicate significant advantages using USAM, especially due to reduced cutting forces compared to the conventional milling process. This causes lower mechanical loads on the tool and surface, combined with lower tensile residual stresses on and below the surface, and ultimately results in a significantly enhanced surface integrity.

1 Introduction

High Entropy Alloys (HEAs) represent a new class of alloys [1, 2], which have become a major focus of materials research. Compared to conventional alloys, they do not have one major alloying element, but at least five different alloying elements with proportions of 5 to 35 at. % [3, 4]. The special feature of HEAs is that they can form a single solid solution phase despite their high number of alloying ele-

ments [1]. HEAs offer the potential to obtain significantly improved properties and property combinations than conventional alloys [5, 6]. Therefore, HEAs are of great interest for many different applications. In this context, the $Co_{20}Cr_{20}Fe_{20}Mn_{20}Ni_{20}$-HEA, the so-called Cantor-alloy, has been investigated the longest and most intensively to date. This CoCrFeMnNi alloy exhibits excellent mechanical properties at very low temperatures. For that reason, especially cryogenic applications are conceivable here, such as pipes or tanks for liquified gases [7].

When using HEAs in real components, it must be ensured that they can be manufactured and processed safely. To date, there are very few publications dealing with the machining of HEA components, and in fact no systematic knowledge about the safe and reliable machinability of these materials [8, 9]. In this regard, machining has a great influence on the safety of components, especially the surface integrity, which is characterized by topography (roughness, defects), mechanics (residual stresses, work hardening) and metallurgy (microstructural changes). It considerably affects the resilience and service life of components in terms of corrosion resistance, crack initiation and propagation (e.g. stress corrosion cracking, fatigue cracking). For hard and brittle materials, e.g. quartz glass and ceramics, very good results have been achieved with innovative hybrid manufacturing processes, such as ultrasonic-assisted grinding, in terms of reducing cutting forces and increasing surface quality and which are already state of the art in production [10]. This has already been transferred to various metallic materials that are difficult to machine using tools with geometrically defined cutting edges. In case of ultrasonic-assisted milling (USAM) of NiCr-alloys, very good results have already been achieved in terms of increased surface integrity and reduced cutting forces, temperatures and tool wear [11-14]. Nonetheless, systematic knowledge is rare so far, especially when using radius cutters for finishing of complex components.

In this work, finish milling processes using ball nose end milling tools on a CoCrFeMnNi alloy are therefore being investigated for the first time and compared with ultrasonic-assisted milling processes. The aim is to obtain essential findings for reliable and safe machining of these innovative high-performance materials.

2 Experimental

2.1 Material preparation

The CoCrFeMnNi alloy, produced by cooperation partners of the Ruhr-University Bochum, was used for the milling tests. This alloy is already widely represented in the literature with regard to production and properties [2, 7, 15-18]. The material was melted with a vacuum induction furnace in an aluminum crucible made of elements with a purity of 99.9 wt.% and then homogenized at 1200 °C for 48 h. The diameter of the ingots could be reduced from 40 mm to 17 mm by rotary forging, followed by recrystallisation annealing at 1020 °C for 60 min, as explained in detail in [19]. As a result, the alloy shows a pure face-centered cubic phase with a grain size of ~50 µm and some Cr- and Mn-rich oxides [18, 20]. In the literature , the yield strength (273 MPa) and the ultimate tensile strength (633 MPa) are given for a similar material condition at room temperature [18]. The chemical composition was measured with an electron microprobe, cf. table 1.

Table 1. Chemical composition of CoCrFeMnNi alloy.

Element	**Co**	**Cr**	**Fe**	**Mn**	**Ni**
Atm. %	19.7	20.7	19.6	20.1	19.9

2.2 Milling experiments

For the milling experiments, the ingot was separated perpendicular to the axial direction by electrical discharge machining (EDM) and slices of approx. 2 mm thickness were produced. The experiments were conducted at the 5-axis machining center DMU 65 of Sauer GmbH/DMG MORI, modified for USAM. The experimental setup for finishing milling using solid carbide end mills with full radius (diameter 6 mm) is shown in figure 1a. The special carbide tool was designed by the manufacturer (WOLF Werkzeugtechnologie GmbH) for use on difficult-to-machine alloys in accordance to DIN 6527L with

four flutes and PVD coating with TiAlSiN [21]. The specimens were milled under dry condition (without cooling lubricant) in down milling mode and the tool was tilted in the primary (*x*) and secondary feed direction (*y*-direction), see figure 1a.

A full-factorial design of experiments was used for parameter variation, see figure 1b. In addition to the ultrasonic assistance, the cutting speed v_c and the feed rate per cutting edge f_z have been varied in accordance to the specifications of the tool manufacturer.

a)

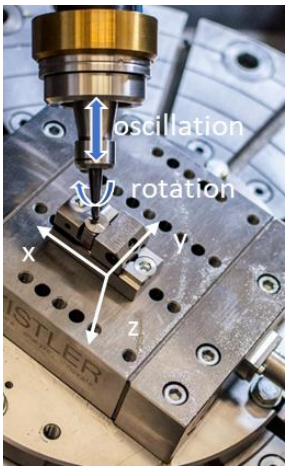

b)

angle in x-direction $\lambda = 45°$			**step over** $a_p = 0.3$ mm				**ultrasonic frequency** $f_{US} = 39.7 \pm 0.2$ kHz			
angle in y-direction $\tau = 45°$			**cutting engagement** $a_e = 0.3$ mm							
test no.	1	2	3	4	5	6	7	8	9	10
v_c in m/min	30	30	110	110	70	30	30	110	110	70
f_z in mm	0.04	0.07	0.07	0.04	0.055	0.04	0.07	0.07	0.04	0.055
USAM in %	0	0	0	0	0	100	100	100	100	100

Figure 1. (a) experimental setup, (b) experimental data.

Various investigations were carried out to characterize the surface integrity of the milled surfaces. Statements about the topography could be derived by means of light microscopic as well as SEM examinations. In addition, the roughness in *x*- and *y*- direction was measured with a contact profile meter according to DIN EN ISO 4287 [22]. The metallurgical influence and its depth could be investigated by means of SEM examinations perpendicular to the machined surface.

2.3 Force measurement

During the milling experiments the cutting forces in *x*- (F_f - feed force), *y*- (F_{fN} - normal feed force) and *z*-direction (F_p - passive force) were measured with a dynamometer from Kistler with a resolution of 0.1 ms, see figure 1a. To describe the acting force, the resulting cutting force F_r is calculated according to equation 1:

$$F_r = \sqrt{{F_f}^2 + {F_{fN}}^2 + {F_p}^2} \qquad (1)$$

2.4 Residual stress determination

To evaluate the mechanical effects of milling on the surface and the process related loads, principal residual stress analyses were carried out using X-ray diffraction (XRD, penetration depth approx. 5 µm, G3 Stresstech Goniometer). The determination of a residual stress profile in depth direction could be achieved by multiple electrochemical polishing. For this purpose, after each polishing step a stress measurement was carried out down to a depth of 40 µm. The electrochemical polishing was performed with a voltage of 25 V for 5 s, whereby a layer of approx. 5 µm was removed. The parameters for the XRD measurements are given in table 2. The calculation of the residual stresses is based on the material data from the literature [15] with Poisson's ratio υ (0.259) and Young's modulus *E* (207 GPa).

Table 2. X-ray measuring and evaluation parameters.

Measuring mode	$\sin^2\psi$	Collimator ⌀	3 mm
Radiation	Mn-Kα	Tube power	30 kV/ 6.7 mA
Detector	Linear solid-state detector	ψ – tilting	0° bis ± 45°
Diffraction line	(311)	ψ - step	9
2Θ angel	156°	Measuring time	2 s

3 Results

3.1 Forces during milling

During the milling tests, the cutting forces F_f, F_{fN}, F_p were measured and the resulting cutting force F_r was calculated. The measured cutting forces are shown exemplarily in figure 2a and b. The resulting cutting force is shown in figure 2c for a milling test and its relation to the partial forces in figure 2d. The respective peaks can be assigned to one cutting action of the tool so that four peaks occur during one tool revolution. To compare the individual force measurements, the average of the individual peak maxima of the resulting cutting force $F_{r,max}$ is used in the following.

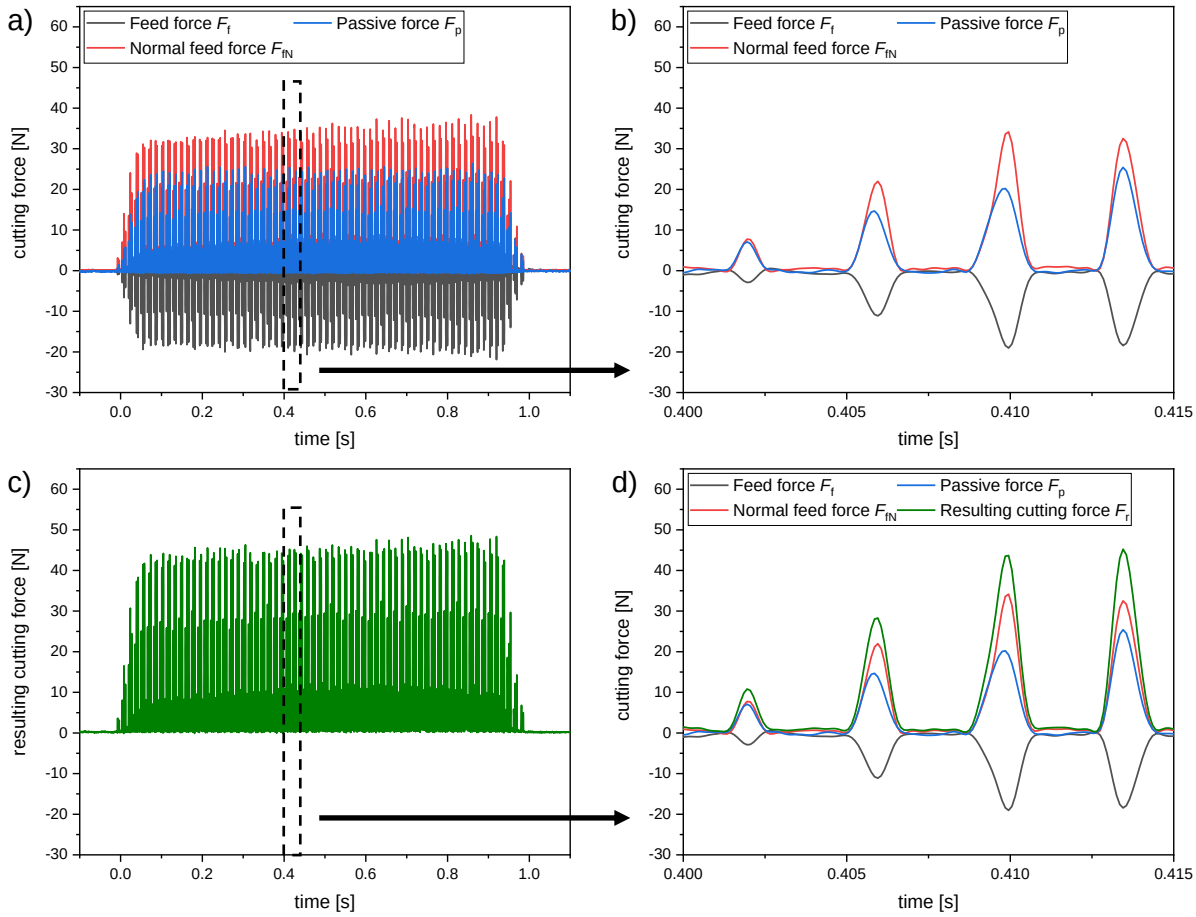

Figure 2. (a) Force measurement for one milling experiment, (b) for one tool revolution (n=1), (c) resulting cutting force and (d) calculated resulting cutting force for one tool revolution (n=1).

Differences in the cutting force maxima stem from the normal manufacturing deviation of the individual cutting edges of the newly used tool. Therefore, it should be noted that due the lower feed rate per cutting edge and cutting engagement commonly used for finish milling the cutting edges are not all equally engaged.

To show the influence of the ultrasonic assistance on the cutting forces, the force measurements of test no. 5 and test no. 10 (see figure 1b) are compared in figure 3.

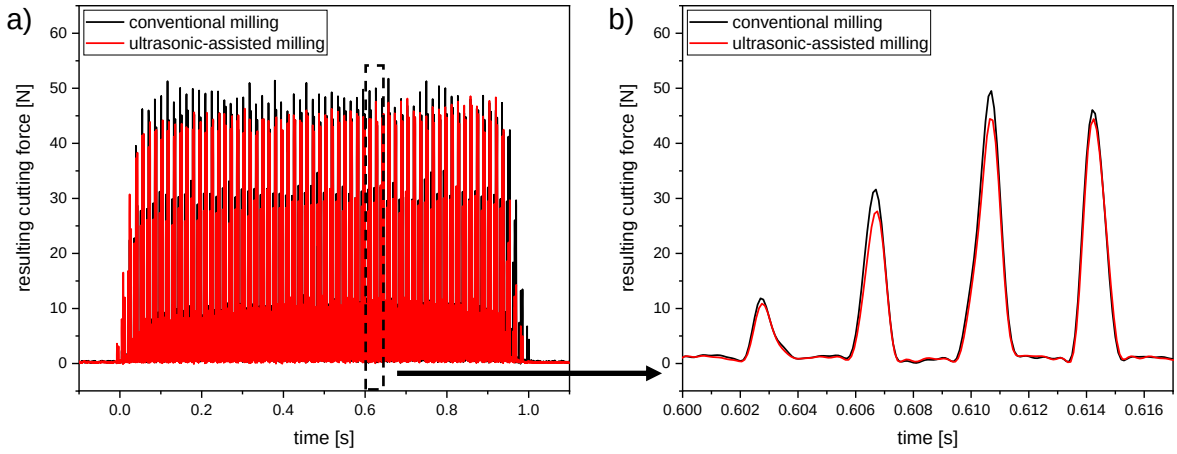

Figure 3. Comparison of the resulting cutting forces of conventional (test no. 5) and ultrasonic-assisted (test no. 10) milling of a test (a) and a tool revolution (b).

Figure 3b shows that the maximum resulting cutting force with ultrasonic assistance is lower as in conventional milling. This can be seen from the lower peak maximum of the resulting cutting force for all four cutting edges. The main reason for the reduced cutting forces is a reduced contact time due to the additional relative movement of the ultrasonic oscillation (superposition principle) with a frequency of approx. 40 kHz exceeding the cutting frequency of the individual cutting edges [23]. In addition, the coefficient of friction between tool and material surface decreases due to this high-frequency tool oscillation and causes a reduction of the cutting forces.

The influence of the milling parameters on the resulting cutting force is shown in figure 4a (f_z – feed rate per cutting edge) and b (v_c – cutting speed) for conventional and ultrasonic-assisted milling. Figure 4a shows that the resulting cutting force decreases by 38 % as the feed rate per cutting edge decreases. The cutting speed in figure 4b also has a highly significant influence on the cutting force. Within the given parameters, the cutting force can be reduced by approx. 28 % by increasing the cutting speed from 40 m/min to 110 m/min. From this, a clear influence of the feed rate per cutting edge and the cutting speed on the mechanical loads for workpiece and tool and thus on the surface integrity and service life of the tools can be concluded [24]. A comparison of conventional and ultrasonic-assisted milling shows a reduction of the resulting cutting force by approx. 5 % due to the ultrasonic assistance, for the complete parameter matrix, independently of feed rate and cutting speed, cf. figure 3. Thus, an overall positive effect of the ultrasonic assistance on the tool load can be observed. Even for such comparably small reductions of the process induced loads, distinct beneficial effects were identified considering the surface integrity, see section 3.2. From that it can be stated, that ultrasonic assistance is at least showing potential for an expansion of the working ranges in terms of machining without increasing the load.

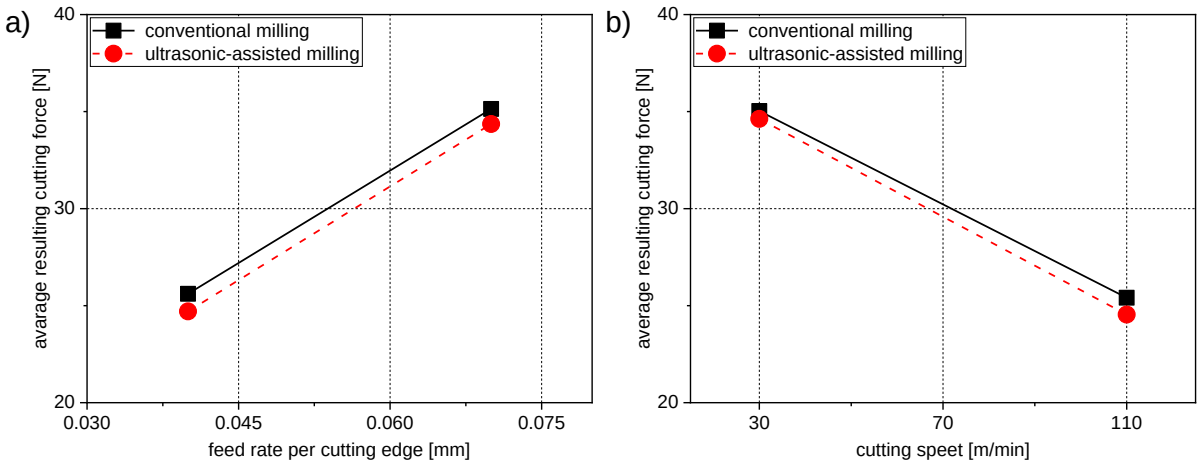

Figure 4. Influence of the milling parameters on the resulting cutting force: feed rate per cutting edge f_z (average over all v_c) (a) and cutting speed v_c (average over all f_z) (b).

3.2 Surface integrity

In order to discuss the influence of ultrasonic assistance on the surface integrity in detail, the specimens of milling tests no. 2 and no. 7 (see figure 1b) were assessed in this study, see figure 1b. These milling tests provide the highest mechanical load on the tool that was observed in the complete parameter matrix (high f_z and low v_c), cf. section 3.1. In this context, a distinct influence of USAM application was expected.

3.2.1 Topography. The topographies of conventional (a-c) and ultrasonic-assisted (d-f) machining are compared in figure 5. The light microscopic observations (a, d) show a typical milling pattern. The shape of the pattern depends mainly on the milling parameters such as the feed rate per cutting edge, the step width or the angle of inclination. In addition, figure 5a shows the influence of the manufacturing deviation of the tool (see Section 2.3) based on milling cuts of different widths. Furthermore, this figure shows milling marks which are at an angle of 45° to the feed direction x due to the double tool tilt. They are the result of the tool micro geometry and the adhesion [25]. In figures 5d, e and f, the ultrasonic pattern are visible perpendicular to the milling marks comparable to waves on a surface. These are caused by the ultrasonic oscillation of the tool. Since the ultrasonic frequency of approx. 40 kHz exceeds the cutting frequency of approximately 111 Hz (for test no. 2 and 7) by several hundred times, multiple of these ultrasonic patterns can be detected per cut, in accordance with the superposition principle.

Figures 5b and e show defects on both conventional and ultrasonic-assisted milled surfaces, which are abrasive marks and chipping of Cr and Mn oxides ($(Cr,Mn)_3O_4$). These hard oxides, present in the CoCrFeMnNi alloy [20], are ground by the cutting edge over the fresh formed surface and cause a groove due to the abrasive effect of the oxides [26]. In addition, the SEM images of conventionally milled surfaces in figure 5b and c reveal further defects. These are similar to the so-called tear defects, cf. morphology in figure 5c. Tear defects are the most common machining-related surface defects in nickel-based materials such as Inconel 718 and are usually the result of insufficient cutting speed [27, 28]. One reason for this is for instance the formation of a built-up edge in combination with unfavorable milling parameters (e. g. low cutting speed) and hard particles, such as NbC-precipitates in Inconel 718. However, the defect mechanism cannot be clearly clarified with the presented results. This kind of defects were not detected on the surface machined with USAM. For this reason, it is anticipated that such defects can effectively be avoided with USAM.

The previously described local defects can also act as initiation points for pitting corrosion or notches for crack initiation, thus reducing the surface integrity of CoCrFeMnNi alloy components [29]. Tear defects can be consistently avoided by use of ultrasonic assistance and adapted milling parameters. The

oxide-related grooves, on the other hand, must be considered by adjusting the process parameters during material production to suppress such hard oxide inclusions in the microstructure.

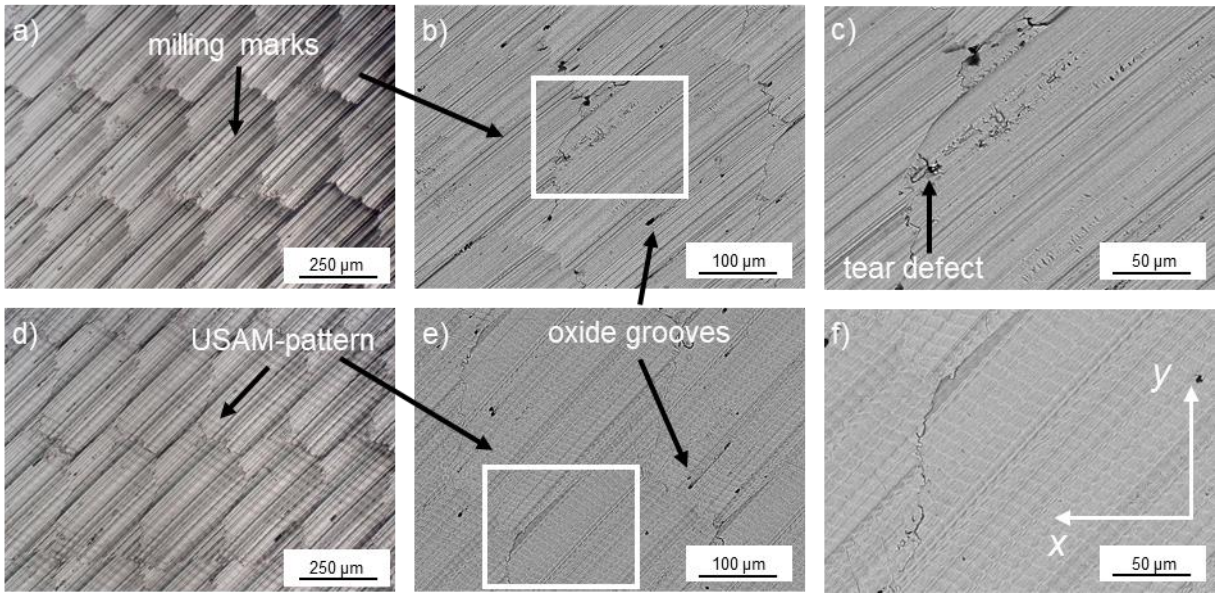

Figure 5. Comparison of the topography of conventional milling (a-c; test no. 2) and USAM (d-f; test no. 7) with light microscope (a, d) and SEM (b, c, e, f).

In comparison to the qualitative evaluation by optical light microscopy and SEM, the topography can be described quantitatively by determining the roughness values. The measured roughness values R_a (arithmetical mean deviation) and R_z (maximum profile height) are shown in table 3. There are no significant effects on the roughness values obvious within the examined test matrix if USAM is compared to conventional milling. In the secondary feed direction (y), the roughness values are higher than in the feed direction (x), which is due to the penetration kinematics or kinematic topography between the tool cutting edge and the material. This interdependency is determined by the tool macro geometry, the feed rate per cutting edge f_z, the step over a_p and the angles of inclination λ, τ [30, 31].

With an arithmetical mean deviation between 0.9 µm and 0.6 µm, the machining process can be classified in the transition between finishing and fine finishing ($R_a \leq 0.8$ µm) and thus fulfils the requirements placed on the surface of a highly corrosive and mechanically exposed component with safety relevance [32].

Table 3. Comparison of the surface roughness of conventional and ultrasonic-assisted milling using the arithmetical mean deviation R_a (a) and the maximum high of the profile R_z (b).

	Conventional milling	USAM
R_a in x – direction in µm	0.87 ± 0.10	0.88 ± 0.14
R_a in y – direction in µm	0.71 ± 0.29	0.68 ± 0.19
R_z in x – direction in µm	3.61 ± 1.12	3.60 ± 0.70
R_z in y – direction in µm	4.50 ± 0.49	4.65 ± 0.55

3.2.2 Mechanics. Process-related loads caused by milling are principally the mechanical influences, which cause residual stresses in the surface. The residual stress condition has a strong influence on the surface integrity in terms of crack initiation and propagation on the surface. For this purpose, the residual stresses were analyzed by means of X-ray diffraction at and up to 40 µm below the surface and the maximum (principal) residual stresses were determined. The results of the residual stress measurements are shown in figure 6 by means of depth profiles of the maximum residual stresses. It is obvious that for both processes a tensile residual stress level of more than 300 MPa is present at the surface. Thus, the tensile residual stresses on the surface approximately correspond to the strength of the material

(273 MPa [18]), due to plastic deformation and local temperature gradients while cutting [33]. However, the decrease of the tensile residual stresses of the USAM-specimen is comparatively greater with the distance from the surface. While the residual stresses in USAM are approximately 0 MPa at about 15 µm below the surface and change to compressive residual stresses in greater depth, a tensile residual stress level of approx. 200 MPa is present for conventional milling down to a depth of 20 µm. In addition, tensile residual stresses of about 100 MPa are still present in the conventionally milled sample down to a depth of about 40 µm below the surface.

The higher tensile residual stresses in the conventionally milled specimens can support crack formation and propagation, thus increasing the risk of component failure. From a stress-related point of view, the USAM shows a significantly higher surface integrity than the conventionally milled specimen. This makes USAM more suitable for safety-relevant components by its generation of smoother surface. That can withstand stress corrosion cracking in severe environments better or generally increased fatigue cracking resistance by avoiding mechanical notches compared to conventional milling.

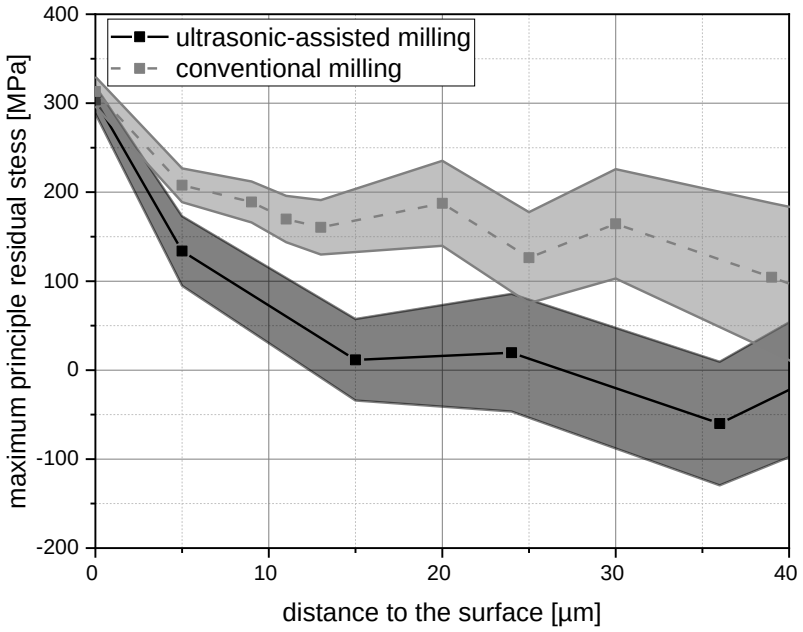

Figure 6. Influence of conventional and ultrasonic-assisted machining on the residual stresses at and below the surface.

3.2.3 Metallurgy. The metallurgical influence is mainly characterized by microstructural degradation in the area of the surface. The surface integrity highly depends on the properties and the prevailing microstructure. For this purpose, specially prepared cross sections of the milled surfaces (test no. 2 and 7) were examined by SEM, see figure 7. Shear bands in the area below the surface reveal in both the conventionally milled and the USAM-sample. A pronounced appearance of these shear bands indicates a high deformation during milling. Compared to USAM (figure 7b), the shear bands are more evident in conventional milling (figure 7a) and, at up to about 9.3 µm, extend approx. 30 % deeper under the machined surface. In these highly deformed areas, a mechanically significantly degraded microstructure can be assumed in connection with pronounced grain refinement and orientation. In this context, it can therefore be assumed that for instance the risk of crack initiation will be reduced due to the lower metallurgical influence of USAM process. These results confirm the findings of the authors [34] for the USAM of Ti-6Al-4V with higher feed rates per cutting edge and in this connection the residual stress analyses in section 3.2.2.

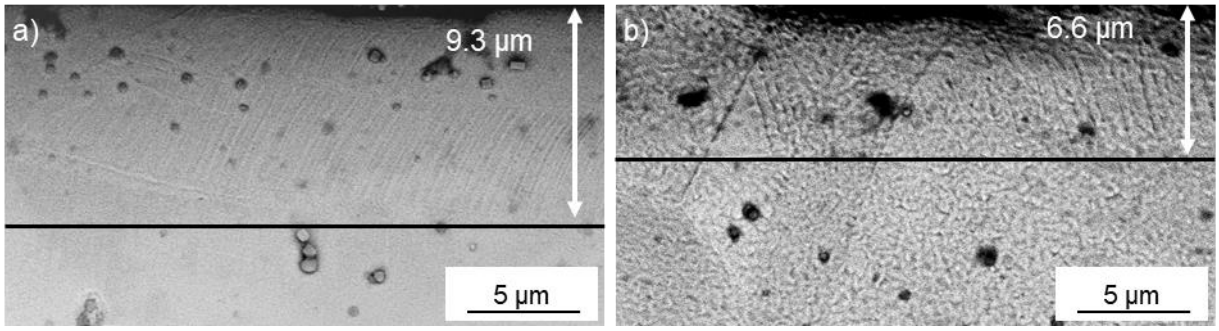

Figure 7. SEM images perpendicular to the surface from conventional (a) and ultrasonic-assisted milling (b).

The results in figure 7 reflect the results of the force evolution (sections 3.1), the topography (section 3.2.1) and the mechanical effect (section 3.2.2) with an increased surface integrity by USAM well. Here, the increased mechanical loads from conventional machining due to increased cutting forces from section 3.1 show a clear effect on the surface integrity of the CoCrFeMnNi alloy. The lower cutting forces and contact times of the tool cutting edges with the surface lead to a reduction in local overloading on the material surface in the USAM. This prevents local microdefects and increases the overall surface integrity.

Finally, the results show that the investigated CoCrFeMnNi alloy is comparatively well machinable with the carbide milling tool used. The machining process and the resulting surface integrity can be further optimized with ultrasonic assistance, respectively the working range for machining parameters can be extended if applying USAM. However, the influence of microdefects caused by oxide inclusions must be considered.

4 Summary and conclusion

In this study, the experimental results on the influence of conventional and ultrasonic-assisted finishing milling processes using ball nose end mills on a CoCrFeMnNi alloy are presented. The investigations focused on the cutting process, the cutting forces and the resulting surface integrity of the milled HEA samples. The surface integrity was characterized by the topography and the mechanical and microstructure. The following conclusions can be drawn from this study:

- The investigated CoCrFeMnNi alloy can be safely machined with the solid carbide radius cutter used. The resulting cutting force can be significantly reduced by adjusting the milling parameters. The cutting force could be reduced within the scope of the test matrix by lowering the feed rate per cutting edge by about 38 % and by increasing the cutting speed by about 28 %. Furthermore, the resulting cutting force can be reduced significantly by about 5 % on average for the entire test matrix by means of ultrasonic-assisted machining.
- The surface integrity of the CoCrFeMnNi alloy can be significantly improved compared to conventional milling with ultrasonic assistance. This is demonstrated by a reduction of microdefects on the surface, lower tensile residual stresses at or below the surface and a lower and less in-depth metallurgical influence.
- The HEA CoCrFeMnNi is comparatively well machinable with the applied milling tool and the selected boundary conditions (plane-finish milling) and milling parameters. High quality surfaces could be produced by the finishing milling processes. Further investigations will be carried out to determine the extent to which these surfaces can withstand mechanical, thermal and corrosive loads or combinations of loads. For this purpose, the influence of machining production steps on the corrosion properties and crack initiation of the alloy CoCrFeMnNi will be investigated further.

Acknowledgements
The authors want to thank Prof. Guillaume Laplanche and co-workers from Ruhr-University Bochum, Germany, for providing the experimental materials and WOLF Werkzeugtechnologie GmbH for providing milling tools.

References
[1] Yeh J W, Chen S K, Lin S J, Gan J Y, Chin T S, Shun T T, Tsau C H,Chang S Y, 2004 Advanced Engineering Materials **6** 299-303.
[2] Cantor B, Chang I T H, Knight P,Vincent A J B, 2004 Materials Science and Engineering: A **375-377** 213-218.
[3] Miracle D B,Senkov O N, 2017 Acta Materialia **122** 448-511.
[4] Gorsse S, Miracle D B,Senkov O N, 2017 Acta Materialia **135** 177-187.
[5] Pickering E J,Jones N G, 2016 International Materials Reviews **61** 183-202.
[6] Zhang Y, Zuo T T, Tang Z, Gao M C, Dahmen K A, Liaw P K,Lu Z P, 2014 Progress in Materials Science **61** 1-93.
[7] Otto F, Dlouhý A, Somsen C, Bei H, Eggeler G,George E P, 2013 Acta Materialia **61** 5743-5755.
[8] Guo J, Goh M, Zhu Z, Lee X, Nai M L S,Wei J, 2018 Materials & Design **153** 211-220.
[9] Polishetty A, Barla M M R, Littlefair G,Fabijanic D, 2015 International Conference on Manufacturing Engineering and for Manufacturing Growth Vancouver **3** 41-44
[10] Kumar M N, Subbu S K, Krishna P V,Venugopal A, 2014 Procedia Engineering **97** 1577-1586.
[11] Suárez A, Veiga F, de Lacalle L N L, Polvorosa R, Lutze S,Wretland A, 2016 Journal of Materials Engineering and Performance **25** 5076-5086.
[12] Ahmed N, Mitrofanov A V, Babitsky V I,Silberschmidt V V, 2006 Materials Science and Engineering: A **424** 318-325.
[13] Chen W, Huo D, Shi Y,Hale J M, 2018 The International Journal of Advanced Manufacturing Technology **97** 2033-2049.
[14] M'Saoubi R, Outeiro J C, Chandrasekaran H, Jr. O W D,Jawahir I S, 2008 Int. J. Sustainable Manufacturing **1** 203-236.
[15] Zaddach A J, Niu C, Koch C C,Irving D L, 2013 Jom **65** 1780-1789.
[16] Schuh B, Mendez-Martin F, Völker B, George E P, Clemens H, Pippan R,Hohenwarter A, 2015 Acta Materialia **96** 258-268.
[17] Gludovatz B, George E P,Ritchie R O, 2015 Jom **67** 2262-2270.
[18] Wu Z, David S A, Leonard D N, Feng Z,Bei H, 2018 Science and Technology of Welding and Joining **23** 585-595.
[19] Laplanche G, Berglund S, Reinhart C, Kostka A, Fox F,George E P, 2018 Acta Materialia **161** 338-351.
[20] Schulz W, Laplanche G, Schneider M, Karafiludis S,Stephan-Scherb C, 2020 Oxidation of Metals **to be published**.
[21] DIN-6527L, Vollhartmetall-Schaftfräser mit abgesetztem Zylinderschaft-Maße, Beuth publishing DIN, 2002
[22] DIN EN ISO 4287, Geometrische Produktspezifikation (GPS) - Oberflächenbeschaffenheit: Tastschnittverfahren - Benennungen, Definitionen und Kenngrößen der Oberflächenbeschaffenheit, Beuth publishing DIN, 2010
[23] Ni C, Zhu L, Liu C,Yang Z, 2018 International Journal of Mechanical Sciences **142-143** 97-111.
[24] Choudhury S K,Rao I V K A, 1999 Int J Mach Tool Manu **39** 343-353.
[25] Grzesik W, 1996 Wear **194** 143-148.
[26] Klocke F,Köning W, Fertigungsverfahren 1, Springer - Verlag, 2008.
[27] Liu C, Ren C, Wang G, Yang Y,Zhang L, 2015 Journal of Mechanical Science and Technology **29** 1723-1730.

[28] Dosbaeva G K, Veldhuis S C, Elfizy A, Fox-Rabinovich G,Wagg T, 2010 Journal of Materials Engineering and Performance **19** 1193-1198.
[29] Roberge P R, Handbook of Corrosion Engineering, McGraw-Hill, 2000.
[30] Vopát T, Peterka J, Šimna V,Kuruc M, 2015 Procedia Engineering **100** 868-876.
[31] Baccar M H, Bayraktar E, Rickert T, Boujelbene M,Katundi D, 2013 Experimental and Applied Mechanics, Volume 4 191-201
[32] Keferstein C P, Marxer M,Bach C, Fertigungsmesstechnik, Springer Vieweg, 2018.
[33] Sharma V,Pandey P M, 2016 Ultrasonics **70** 172-182.
[34] Liu J, Jiang X, Han X, Gao Z,Zhang D, 2018 The International Journal of Advanced Manufacturing Technology **101** 1451-1465.